

# Design and Analysis of a New Piezoelectric MEMS Tilt Sensor

Paul M. Moubarak

Robotics and Mechatronics Laboratory  
Mechanical and Aerospace Engineering  
The George Washington University  
Washington, DC, USA  
e-mail: [paul4@gwu.edu](mailto:paul4@gwu.edu)

Pinhas Ben-Tzvi

Robotics and Mechatronics Laboratory  
Mechanical and Aerospace Engineering  
The George Washington University  
Washington, DC, USA  
e-mail: [bentzvi@gwu.edu](mailto:bentzvi@gwu.edu)

**Abstract**— This paper reports the design and preliminary analytical investigations of a new MEMS piezoelectric tilt sensor. The proposed tilt sensor consists of a Platinum supported beam with a central proof mass which causes the beam to deflect under gravitational loading. This static deflection generates intrinsic stress across the beam, which is a direct function of the dual-axis inclination of the sensor. A thin 0.2  $\mu\text{m}$  layer of Lead Zirconate Titanate ( $\text{PbZrTiO}_3\text{-PbTiO}_3$ ) deposited on the top surface of the beam where the peak stress occurs, enables the conversion of the variable stress as a function of the spatial inclination to a measurable voltage. The voltage output of the PZT layer is therefore directly proportional to the inclination of the sensor around two orthogonal axes. The feasibility of this measurement approach is validated through simulation results for a dual-axis operation range of 0 – 90°. These results further demonstrate the tunable sensitivity property of the sensor as a function of its geometry.

**Keywords**- MEMS, direct piezoelectric effect, tilt sensor, dual-axis inclination

## I. INTRODUCTION

TILT sensors measure the inclination of an object or a surface with respect to a reference axis, most notably with respect to the vertical gravitational field. Measuring tilt angles can traditionally be done as a single axis measurement where only one angular variable is sensed, or as multi-axes measurements such as the dual-axis roll and pitch angles of an aircraft. In the recent decade, interest in tilt sensors has risen considerably with the expansion of their applications beyond the traditional aerospace and automotive market. They are now being widely used in consumer products and electronics, such as video games, cellular phones and computers.

Depending upon the physics that govern their principles of operation, tilt sensors can achieve different levels of accuracy and resolution which are often dictated by their application. Moreover, with the ongoing trend of miniaturization made possible by the sustained development in MEMS materials and fabrication techniques, multiple physics – beyond the traditional solid and liquid pendulum dynamics [1] – have been investigated for the sensing of angular inclination. Such physics can be classified into two major categories. A first category that achieves high accuracy and high resolution

levels, but requires highly advanced instrumentation and fabrication techniques, and a second category that builds on simpler physics at the expense of the high accuracy level.

In the first category, physics such as optics [2] – [5] have been reported to deliver an accuracy and resolution level of up to 300 *prad* [6]. This level of precision is desirable for aerospace and defense applications where the cost of the tilt sensor is normally not a consideration. However, for other applications that do not require this level of accuracy, such as cell phones (the *iPhone* for instance) and computers, where the angular measurement is defined as a range rather than a single accurate value, optical tilt sensors constitute a prohibitively expensive choice of large-size inclinometers technology. Instead, other physics such as piezo-resistivity [7], [8] electrolysis [9] and thermal transport phenomena [10] constitute a more affordable choice. This is because of their smaller-size, instrumentational simplicity and low-cost despite the relatively lower levels of accuracy they can achieve and their inherent susceptibility to external stimuli [11] – [14].

In this line of thought, this paper proposes a novel approach of low-cost dual-axis inclination measurement that relies on a simple suspended MEMS structure governed by simple physics. The proposed sensor is characterized by its micro-size and its tunable sensitivity, where the latter is a direct function of its geometry. The approach is based on the dynamics of stress and deflection induced in suspended beam structures under gravitational static loading. The proposed tilt sensor consists of a 900  $\mu\text{m}$ -long Platinum beam supported on a Silicon substrate with a central cavity. The beam carries a central Platinum proof-mass that causes the suspended structure to deflect under its own weight. This deflection induces intrinsic stress across the beam which varies as a function of the dual-axis inclination of the tilt sensor. A thin 0.2  $\mu\text{m}$  layer of PZT (Lead Zirconate Titanate) deposited on the beam's top surface, where the peak stress occurs, converts the variable stress into a measurable electrical voltage. This creates a piezoelectric tilt sensor whose output is proportional to the roll and pitch angles of the inclined surface.

This paper therefore presents the early investigations pertaining to the proposed new tilt sensor. The mathematical analysis and the governing physics of the sensor are first introduced, and then a CAD model of the sensor with appropriate dimensions is presented. The concept of operation

is further validated through simulations, which characterize the dual-axis output of the sensor along with its tunable sensitivity as a function of its geometry.

## II. MATHEMATICAL ANALYSIS AND CONCEPT OF OPERATION

A schematic of the proposed tilt sensor is shown in Figs 1 and 2. The roll inclination around the  $x$ -axis is defined by an angle  $\beta$  (Fig. 1) and the pitch inclination around the  $z$ -axis is defined by an angle  $\Theta$  (Fig. 2). The proof-mass that the suspended beam carries in the center causes the structure to deflect under its own static weight (Fig. 2). This deflection introduces three-dimensional (XYZ) intrinsic stresses across the beam, which are described by a stress tensor  $T$  with six independent components.

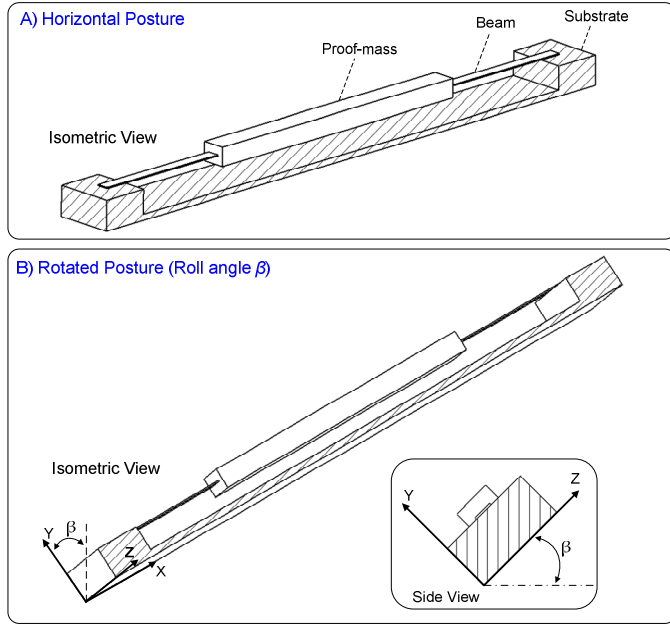


Figure 1. A schematic representation of the tilt sensor in the horizontal posture and the single-axis roll inclination ( $\beta$ -rotation around the  $x$ -axis)

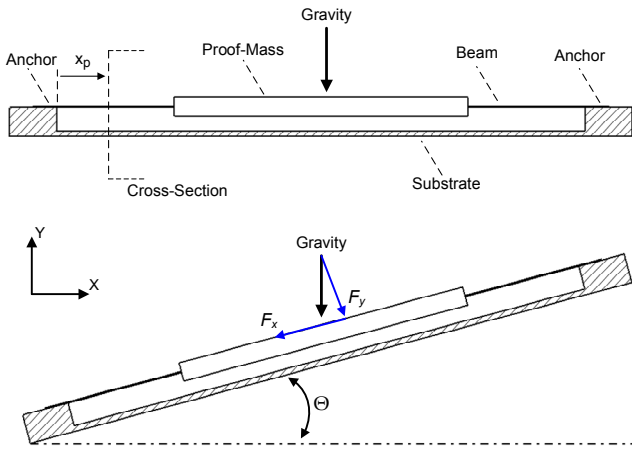


Figure 2. A schematic representation of the tilt sensor in the horizontal posture and the single-axis pitch inclination ( $\Theta$ -rotation around the  $z$ -axis) While tensor  $T$  is traditionally written in a matrix format

in  $\mathbb{R}^{3 \times 3}$  space, it can also be expressed as a vector of the form

$$\mathbf{T} = [T_1 \ T_2 \ T_3 \ T_4 \ T_5 \ T_6]^T \quad (1)$$

where, based on the axes defined in Fig. 2,  $T_1 \triangleq \sigma_x$  denotes the longitudinal stress along the  $x$ -axis,  $T_2 \triangleq \sigma_y$  denotes the vertical stress along the  $y$ -axis,  $T_3 \triangleq \sigma_z$  denotes the lateral stress along the  $z$ -axis,  $T_4 \triangleq \tau_{zy}$  denotes the shear stress in the  $z$ - $y$  plane,  $T_5 \triangleq \tau_{xz}$  denotes the shear stress in the  $x$ - $z$  plane and  $T_6 \triangleq \tau_{xy}$  denotes the shear stress in the  $x$ - $y$  plane.

When the structure shown in Figs. 1 and 2 is rotated in any random combination of angles  $\beta$  and  $\Theta$ , the gravitational load  $F = Mg$  of the structure can be expressed as a vector sum of three force components written in terms of angles  $\beta$  and  $\Theta$  as

$$\begin{aligned} F_x &= F \cos(\beta) \sin(\Theta) \\ F_y &= F \cos(\beta) \cos(\Theta) \\ F_z &= F \sin(\beta) \end{aligned} \quad (2)$$

where  $M$  is the combined mass of the beam and the proof-mass and  $g$  is the gravitational acceleration ( $g = 9.81 \text{ m/s}^2$ ).  $F_x$ ,  $F_y$  and  $F_z$  denote the force components along the  $x$ ,  $y$  and  $z$  directions, respectively. Using equation (2), the components of the stress tensor in (1) can be expressed explicitly in terms of angles  $\beta$  and  $\Theta$ , as follows

$$\begin{aligned} T_1 &= \frac{a_{11} F \cos(\beta) \sin(\Theta)}{A_x} + \frac{a_{12} F \cos(\beta) \cos(\Theta) x_p y_p}{I_z} \\ &\quad + \frac{a_{13} F \sin(\beta) x_p z_p}{I_y} \end{aligned} \quad (3)$$

$$T_2 = \frac{a_{21} F \cos(\beta) \cos(\Theta)}{A_y} \quad (4)$$

$$T_3 = \frac{a_{31} F \sin(\beta)}{A_z} \quad (5)$$

$$T_4 = \frac{a_{41} F \cos(\beta) \cos(\Theta) Q_x}{I_x t_x} \quad (6)$$

$$T_5 = \frac{a_{51} F \sin(\beta) Q_y}{I_y t_y} \quad (7)$$

$$T_6 = \frac{a_{61} F \cos(\beta) \sin(\Theta) Q_z}{I_z t_z} \quad (8)$$

The parameters in equations (3) – (8) are defined as follows:

- $A_x$ ,  $A_y$  and  $A_z$  represent the area of the beam's cross-section orthogonal to the  $x$ ,  $y$  and  $z$  axes, respectively.
- $I_x$ ,  $I_y$  and  $I_z$  are the area moment of inertia of the beam's cross-section around the  $x$ ,  $y$  and  $z$  axes, respectively.

- $Q_x$ ,  $Q_y$  and  $Q_z$  are the first moment of area of the beam's cross-section around the  $x$ ,  $y$  and  $z$  axes, respectively.
- $t_x$ ,  $t_y$  and  $t_z$  are the thickness of the cross-section perpendicular to the corresponding shear and measured with respect to the beam's neutral fiber.
- $x_p$ ,  $y_p$  and  $z_p$  represent the coordinates of the points of interest on the beam, where the calculation of the stress tensor is being performed.

Equations (6), (7) and (8) of the shear stress are expressed according to *Jourawski* formula. In addition, coefficients  $a_{ij}=cte$  are added to the expression of the stress element  $T_i$  for two reasons. First,  $a_{ij}$  accounts for the sign contribution of the corresponding term in the expression of  $T_i$ , thus reflecting the tensile or compressive nature of individual terms. Second,  $a_{ij}$  aggregates all numerical constants relevant to every expression, such as the fraction of  $F$  that effectively contributes to the corresponding term of element  $T_i$ .

Equations (3) – (8) clearly show that the stress components vary across the beam and their profile changes as a function of the inclination and the coordinates  $x_p$ ,  $y_p$  and  $z_p$ . However, from the principles of stress of materials, it is known that at any vertical cross-section of the beam defined by coordinate  $x_p$  (Fig. 2), the peak Von-Mises stress occurs at either the top surface or the bottom surface of the beam [15]. Therefore, a PZT layer deposited on the top surface can convert the peak stress into an electrical polarization  $D$  defined by

$$\mathbf{D}(\beta, \Theta) = d \mathbf{T}(\beta, \Theta) \quad (9)$$

where  $d$  is the matrix of constant piezoelectric coefficients of Lead Zirconate Titanate defined as

$$d = \begin{bmatrix} 0 & 0 & 0 & 0 & d_{15} & 0 \\ 0 & 0 & 0 & d_{24} & 0 & 0 \\ d_{31} & d_{32} & d_{33} & 0 & 0 & 0 \end{bmatrix} \quad (10)$$

The polarization vector  $\mathbf{D}(\beta, \Theta)$  generates an electrostatic field  $E$  across the faces of the PZT layer, which can be expressed according to the expression

$$\mathbf{E}(\beta, \Theta) = \varepsilon^{-1} \mathbf{D}(\beta, \Theta) \quad (11)$$

where  $\varepsilon$  denotes the permittivity matrix of the PZT layer defined as a diagonal matrix of the form

$$\varepsilon = \begin{bmatrix} \varepsilon_{xx} & 0 & 0 \\ 0 & \varepsilon_{yy} & 0 \\ 0 & 0 & \varepsilon_{zz} \end{bmatrix} \quad (12)$$

The average voltage across the piezo layer can then be calculated as a line integral of the dot product between the electrostatic field  $\mathbf{E}(\beta, \Theta)$  and the infinitesimal vector displacement  $d\mathbf{l}$  tangent to path  $C$  as

$$V = \int_C \mathbf{E}(\beta, \Theta) \cdot d\mathbf{l} = E \cdot \hat{n} \|\Delta L\| \quad (13)$$

where  $\hat{n}$  denotes a unit vector in the  $\Delta L$  direction, and  $\|\Delta L\|$  denotes the magnitude of vector  $\Delta L$ . In (13), since the electrostatic field is a function of angles  $\beta$  and  $\Theta$ , the voltage  $V$  will identically depend on the roll and pitch angles. In order to reflect this dependence,  $V \triangleq V_{\beta, \Theta}$  is defined and the dot product in (13) is expanded as follows

$$V_{\beta, \Theta} = \|\mathbf{E}(\beta, \Theta)\| \|\Delta L\| \cos(\hat{e}, \hat{n}) = \lambda \|\mathbf{E}(\beta, \Theta)\| \quad (14)$$

where  $E = \|\mathbf{E}\|$ ,  $\lambda = \|\Delta L\| \cos(\hat{e}, \hat{n})$  and  $\hat{e}$  is a unit vector in the direction of the electrostatic field  $E$ .

This mathematical analysis of the proposed tilt sensor shows that the voltage output of the piezo layer is a direct function of the roll and pitch angles of the structure. In the following section, a CAD model of the tilt sensor is proposed, and the concept of operation as outlined in equation (14) is validated for different inclination scenarios within the full range of operation of  $0 - 90^\circ$ .

### III. CAD MODEL AND SINGLE-AXIS ANALYSIS

#### A. Model Design and FEA Analysis

The model of the tilt sensor proposed in this paper consists of a Platinum beam and a central proof-mass with the dimensions as shown in Figure 3. The beam has an active deflecting length of  $900 \mu\text{m}$  and a total tip-to-tip length of  $980 \mu\text{m}$ . As such, the beam is fixed on each side of the substrate with an anchor whose length is  $40 \mu\text{m}$ . The beam thickness is  $0.2 \mu\text{m}$  and its width along the  $z$ -axis is  $20 \mu\text{m}$ .

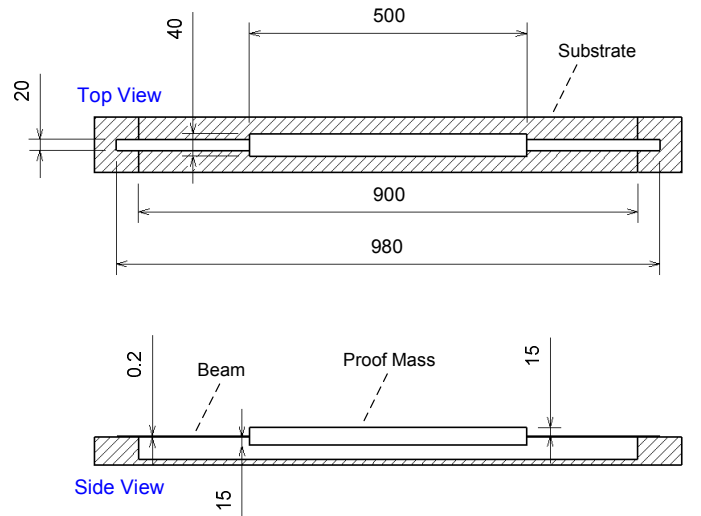


Figure 3. Top and side views of the tilt sensor showing the dimensions of the beam and the proof-mass (dimensions are in  $\mu\text{m}$ )

The proof-mass on the other hand is composed of two Platinum layers each with a thickness of  $15 \mu\text{m}$ . The two layers are symmetric with respect to the beam, which is

cascaded between them. This structural symmetry prevents the creation of eccentric bending moments by aligning the center of mass of the proof-mass with the center of mass of the beam. The length of the proof-mass is 500  $\mu\text{m}$  and its width along the z-axis is 40  $\mu\text{m}$ .

The Platinum material was selected for the proof-mass and the beam for two reasons. First, the high density of Platinum ( $\rho = 21400 \text{ Kg/m}^3$ ) as compared to other MEMS materials (such as Copper ( $\rho = 8900 \text{ Kg/m}^3$ )) generates a large static loading within a small volume. This, along with the selected dimensions of the structure, maintain the miniature size of the device while generating large enough gravitational forces and stresses to increase the sensitivity of the sensor. On the other hand, the high temperatures associated with the deposition of PZT material makes the selection of Platinum a prime choice due to its high melting point ( $1770^\circ \text{ C}$ ).

The beam and the proof-mass are further supported on a Silicon substrate with a cavity etched deep enough to accommodate structural deflections without any interference between the substrate and the proof mass. With these design considerations, dimensions and materials, a CAD model was created and simulated on CoventorWare software as shown in Figure 4. The maximum stress across the beam occurs in the horizontal position at  $\beta = 0^\circ$  and  $\Theta = 0^\circ$ . This is shown in Figure 4 where the cross-section with the peak stress is identified near the anchor points.

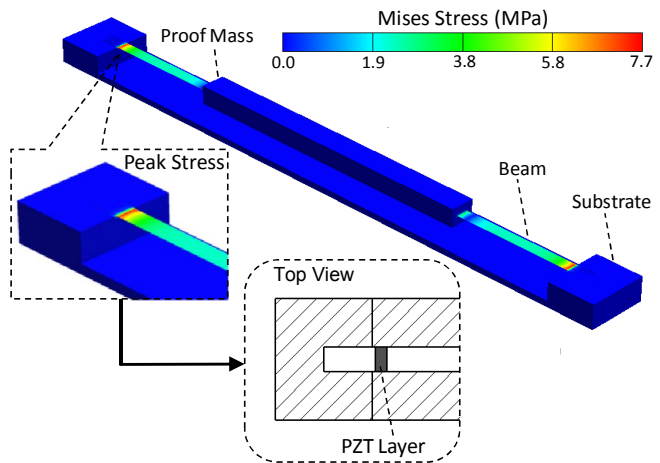


Figure 4. FE stress profile of the sensor model in the horizontal position, with a schematic showing the PZT-layer deposited on the beam's top surface where the peak stress occurs near the anchor points

At this cross-section, a peak stress of 7.2 MPa in the horizontal posture is calculated, which constitutes 6% of the yield strength of Platinum. A PZT layer deposited on the top surface of the beam where this peak stress occurs, allows the conversion of the stress into an electrical voltage. This layer has a footprint of  $10 \times 20 \mu\text{m}$  and a thickness of 0.2  $\mu\text{m}$ .

### B. Single-axis Peak Stress and PZT Voltage Output

To simulate the stress dynamics and the operation of the piezoelectric tilt sensor using the CAD model, we first consider the single-axis operation where one of the angles is held at zero and the other is varied across the range of  $0 - 90^\circ$ . The simulated single-axis stress and voltage profiles are

shown in Figures 5 and 6, respectively. In the case where angle  $\Theta$  is held at zero, the rotation of the sensor is referred to as  $\beta$ -rotation, or rotation around the x-axis. In the other case where angle  $\beta$  is held at zero, the rotation is labeled  $\Theta$ -rotation, or rotation around the z-axis.

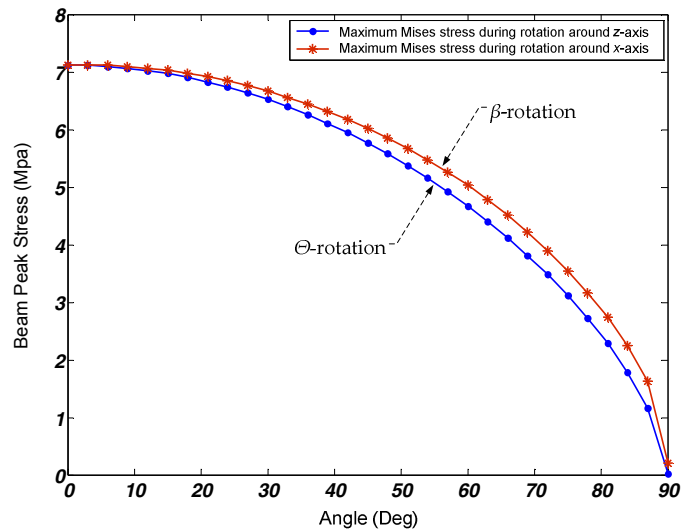


Figure 5. Profiles of the peak stress across the beam as a function of the inclination angle for the single-axis operation (rotation around the x-axis ( $\beta$ ) and rotation around the z-axis ( $\Theta$ ))

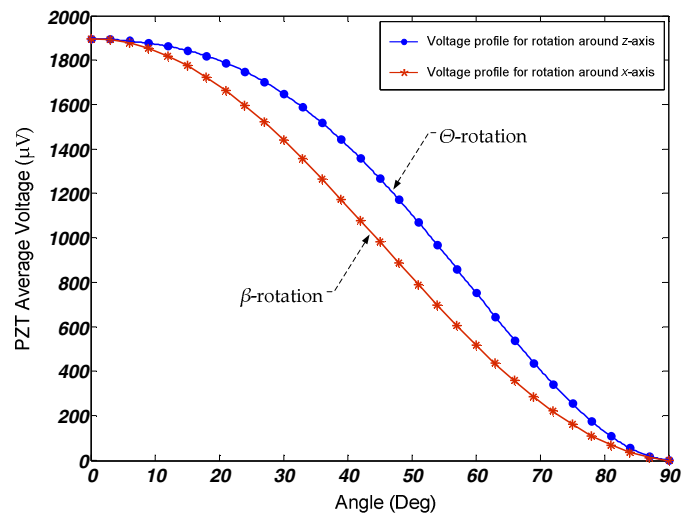


Figure 6. Profiles of the average voltage across the PZT layer as a function of the inclination angle for the single-axis operation (rotation around the x-axis ( $\beta$ ) and rotation around the z-axis ( $\Theta$ ))

The change in the peak stress across the beam as a function of the single-axis inclination angle shown in Figure 5 is in accordance with the stress tensor equations derived in (3) – (8). As can be seen in this figure, the peak stress profile starts at the same maximum at  $\beta = 0^\circ$  and  $\Theta = 0^\circ$  for both single-axis operations, and decreases thereafter towards zero at  $90^\circ$ . This is because the stress shifts gradually away from the beam's top surface to the anchors as the inclination increases, until the sensor reaches the vertical posture where all the stress is carried by the anchors. In each case however, the interpolation between the peak value and the zero value exhibits unique

stress slope characteristics, where the voltage profile relative to the roll rotation ( $\beta$ ) is exclusively distinguishable from the profile corresponding to the pitch rotation ( $\Theta$ ).

The voltage output of the PZT layer corresponding to these stress profiles is shown in Figure 6 for the single-axis operation. The maximum voltage output of the sensor with the dimensions shown in Figure 4 is  $1896 \mu\text{V}$ . The profile for each case also exhibits a unique interpolation between the two extreme values with unique corresponding slope characteristics. This interpolation is delimited by the voltage range of  $1896 - 0 \mu\text{V}$  corresponding to the angular range of  $0 - 90^\circ$ , which translates into a sensor sensitivity of  $21 \mu\text{V}/\text{Deg}$  for the single-axis operation. This sensitivity is a direct function of the sensor geometry as will be discussed in more details in the next section.

#### IV. DUAL-AXIS PARAMETRIC ANALYSIS AND TUNABLE SENSITIVITY

##### A. Dual-axis Analysis

The dual-axis analysis reflects the behavior of the sensor for situations where none of the roll or pitch angles are held at zero. This represents the more general mode of operation where the effect of both angles  $\beta$  and  $\Theta$  is exhibited on the voltage output of the PZT layer. This effect is shown in Figure 7 for selected values of angle  $0 \leq \beta \leq 90^\circ$ , plotted over the full angular range of  $0 \leq \Theta \leq 90^\circ$  in accordance with equation (14).

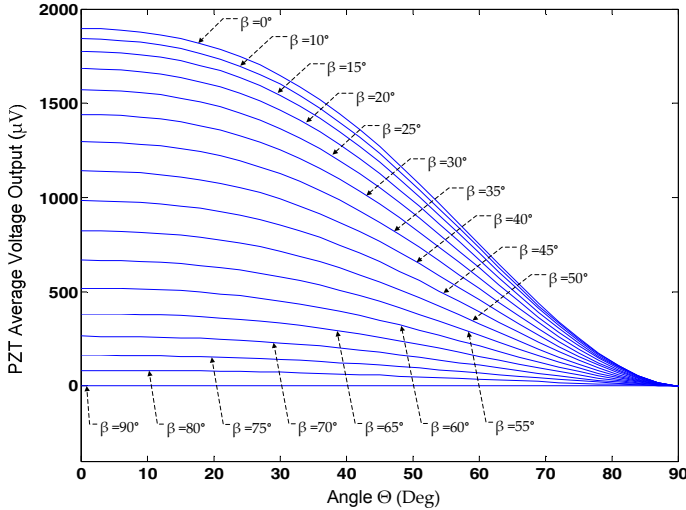


Figure 7. A parametric analysis of the PZT voltage output for the dual-axis full range operation ( $0 \leq \beta \leq 90^\circ$ ,  $0 \leq \Theta \leq 90^\circ$ )

As can be noted in this figure, the peak voltage output corresponding to  $\Theta = 0^\circ$  decreases as a function of angle  $\beta$  until it reaches zero at  $\beta = 90^\circ$ . In fact, the voltage output of the sensor reaches the null value at  $\beta = 90^\circ \forall \Theta$ , as well as at  $\Theta = 90^\circ \forall \beta$ . These postures belong to the null-space of the sensor where a variation in one angle – when the other is held at  $90^\circ$  – creates no variations on the voltage output of the sensor. Outside this null-space, the effect of both angles is noted on the voltage profile (Fig. 7), with the rate of descent (or slope) decreasing with increasing  $\beta$  until the profile reaches a zero-slope at  $\beta = 90^\circ$ .

##### B. Tunable Sensitivity

One main characteristic of the proposed tilt sensor is the dependence of its sensitivity on its geometry. This is because the stress tensor is a direct function of the sensor's dimensions, which influence its structural properties such as the distance separating the center of the gravitational load from the anchors, as well as the area moment of inertia and the first moment of area. This means that the PZT voltage output, and subsequently the sensitivity of the sensor, can be tuned to achieve a desirable sensitivity by selecting appropriate dimensions of the beam and the proof-mass.

To visualize the impact of the sensor's geometry on its voltage output and sensitivity, two scenarios are illustrated in Figs. 8 and 9. Figure 8 shows the correlation between the weight of the structure and the PZT voltage output, and Figure 9 shows the relationship between the beam's length and the PZT voltage.

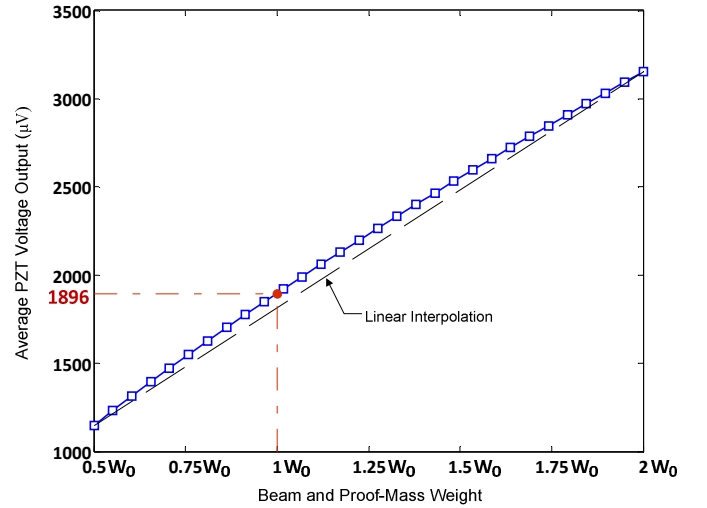


Figure 8. Variation of the PZT voltage output (blue line) at  $\beta = 0^\circ$  and  $\Theta = 0^\circ$  as a function of the beam and proof-mass combined weight ( $W_0$  denotes the weight of the beam and the proof-mass for the sensor dimensions of Figure 3)

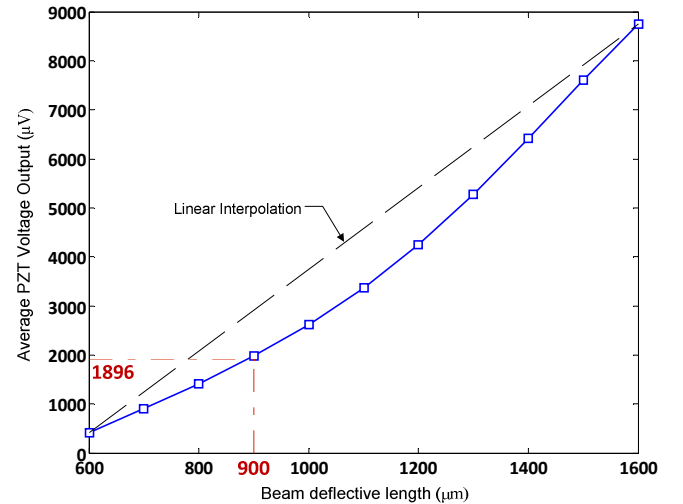


Figure 9. Variation of the PZT voltage output (blue lines) at  $\beta = 0^\circ$  and  $\Theta = 0^\circ$  as a function of the beam's length

As can be seen in these two figures, the voltage output of the PZT layer can be increased by increasing the weight of the structure or the length of the beam. In Figure 8, the relationship between the weight and the PZT voltage is almost linear as compared to the black dashed line, which represents a linear interpolation between the two extremities of the voltage profile (blue solid line).

In Figure 9, the correlation between the beam's length and the PZT voltage is rather non-linear. However, the impact of the increased length on the PZT voltage output is more significant. By comparing Figs. 8 and 9, it can be observed that doubling the length of the beam increases the voltage output of the sensor and thus its sensitivity by ~500%. On the other hand, doubling the weight of the structure without increasing the length of the beam can only increase the PZT voltage output and its sensitivity by ~63%.

## V. CONCLUSION

In this paper, we presented the preliminary analytical and simulation results of a new piezoelectric dual-axis MEMS tilt sensor. The tilt meter proposed in this paper consists of a suspended Platinum beam with a central proof-mass. Under gravitational loading, a stress profile is generated across the beam with a distribution that reaches a peak value near the vicinity of the anchors. This stress profile changes as a function of the roll and pitch angles of the sensor. Thus, a PZT layer deposited on the top surface of the beam where the peak stress occurs, converts the variable stress into a measurable voltage. This voltage is shown to vary as a function of the dual-axis inclination of the sensor over the operation range of 0–90°, with a sensitivity that is a direct function of the sensor's geometry.

The work reported in this paper constitutes the basis of our future investigations, where we plan to examine a new methodology for modeling the direct effect of piezoelectricity using the proposed sensor as a case-study. The objective of such work is to model the dual-axis behavior of the sensor as a function of its single-axis data. The significance of this methodology lies in its independence of the sensor's geometry and structural property. This allows the calibration of the sensor to compensate for drift and fluctuations in the measurements induced by external stimuli known to affect the performance of piezoelectric materials, such as temperature, aging, and depolarization.

Furthermore, our future investigations will also address the inverse sensing problem, where angles  $\beta$  and  $\theta$  are numerically calculated from the self-calibrating model for a given voltage output of the sensor. This will require the derivation of a supplementary equation generated from an additional piezo layer in order to guarantee the uniqueness of the inverse solution. For this, the design of the sensor proposed in Figs. 1 and 2 will be symmetrically modified to include an additional beam orthogonal to the current one, where the additional PZT layer will be deposited.

## ACKNOWLEDGMENT

The authors wish to thank the Chairman of the Electrical Engineering Department, Prof. Mona Zaghoul, for her

guidance and for allowing us to use the department's software (CoventorWare) in their computer facility.

## REFERENCES

- [1] Q. Han, and C. Chen, "Research on Tilt Sensor Technology," *IEEE International Symposium on Knowledge Acquisition and Modeling Workshop, KAM 2008, China, 2008*, pp. 786 – 789.
- [2] X. Dong, C. Zhan, K. Hu, P. Shum, and C.C. Chan, "Temperature-Insensitive Tilt Sensor with Strain-Chirped Fiber Bragg Gratings," *IEEE Photonics Technology Letters*, vol. 17, no. 11, pp. 2394 – 2396, November 2005.
- [3] S. Iqbal, and A. Anand, "Characterization of Multipoint Diffraction Strain and Tilt Sensor based on Moiré Interferometer and Multichannel Imaging Position-Sensitive Detector," *Review of Scientific Instruments*, vol. 77, no. 11, pp. 113110 – 113110-6, November 2006.
- [4] H.Y. Au, S. K. Khijwania, H.Y. Fu, W.H. Chung, and H.Y. Tam, "Temperature-Insensitive Fiber Bragg Grating Based Tilt Sensor With Large Dynamic Range," *J. Lightwave Technology*, vol. 29, no. 11, pp. 1714 – 1720, June 2011.
- [5] B-O. Guan, H-Y Tam, and S-Y Liu, "Temperature-independent fiber Bragg grating tilt sensor," *IEEE Photonics Technology Letters*, vol. 16, no. 1, pp. 224 – 226, January 2004.
- [6] M. Berutto, M. Ortolano, F. Periale, and A. De Marchi, "Realization and Metrological Characterization of a Compact High-Resolution Pendulum Tiltmeter," *IEEE Sensors*, vol. 5, no. 1, pp. 26 – 31, February 2005.
- [7] L. Tang, K. Zhang, S. Chen, G. Zhang and G. Liu, "MEMS Inclinometer Based on a Novel Piezoresistor Structure," *J. Microelectronics*, vol. 40, no. 1, pp. 78 – 82, January 2009.
- [8] U. Mescheder, and S. Majer, "Micromechanical Inclinometer," *J. Sensors and Actuators*, vol. 60, pp. 134 – 138, 1997.
- [9] H. Jung, C.J. Kim, and S.H. Kong, "A MEMS-Based Electrolytic Tilt Sensor," *Proceedings of the 5<sup>th</sup> IEEE Conference on Sensors*, Korea, 2006, pp. 1199 – 1202.
- [10] D.W. Jung, J.C. Choi, J.K. Lee, H. Jung, and S.H. Kong. "Sensitivity Improvement of MEMS-Based Tilt Sensor Using Air Medium," *Proceedings of the 8<sup>th</sup> IEEE Conference on Sensors*, New Zealand, 2009, pp. 164 – 167.
- [11] J-H. Zhang, Q-A. Huang, H. Yu, J. Wang, S-Y. Lei, "Effect of Temperature and Elastic Constant on the Piezoresistivity of Silicon Nanobeams," *J. Applied Physics*, vol. 105, no. 8, pp. 086102 – 086102-3, April 2009.
- [12] R.A. Wolf, and S. Trolier-McKinstry, "Temperature Dependence of the Piezoelectric Response in Lead Zirconate Titanate Films," *J. Applied Physics*, vol. 95, no. 3, pp. 1397 – 1397-10, February 2004.
- [13] G. Xu, X. Wang, D. Yang, Z. Duan, C. Feng, and K. Chen, "Peculiar Temperature Aging Effects on the Piezoelectric Constant of Pb(Mg<sub>1/3</sub>Nb<sub>2/3</sub>)O<sub>3</sub>-PbTiO<sub>3</sub> Single Crystal Near the Morphotropic Phase Boundary," *J. Applied Physics Letters*, vol. 86, no. 3, pp. 032902 – 032902-3, January 2005.
- [14] S. Pruvost, G. Sebald, L. Lebrun, and D. Guyomar, "Depolarization mechanism under compressive stress in Pb(Mg<sub>1/3</sub>Nb<sub>2/3</sub>)<sub>1-x</sub>Ti<sub>x</sub>O<sub>3</sub>," *J. Applied Physics*, vol. 102, no. 6, 064104 – 064104-6, September 2007.
- [15] N. Dowling, *Mechanical Behavior of Materials*, New Jersey: Prentice Hall, 2007, ch. 13.